Agricultural and Forest Meteorology 149 (2009) 2082–2097

Contents lists available at ScienceDirect

Agricultural and Forest Meteorology

journal homepage: www.elsevier.com/locate/agrformet

An intercomparison of three remote sensing-based surface energy balance algorithms over a corn and soybean production region (Iowa, U.S.) during SMACEX

Minha Choi [a,1], William P. Kustas [b,*], Martha C. Anderson [b], Richard G. Allen [c], Fuqin Li [d], Jeppe H. Kjaersgaard [c]

[a] Department of Civil and Environmental Engineering, Hanyang University, Seoul 133-791, Republic of Korea
[b] U.S. Department of Agricultural, Agricultural Research Service, Hydrology and Remote Sensing Laboratory, Beltsville, MD 20705, USA
[c] Kimberly Research Center, University of Idaho, Kimberly, ID 83341, USA
[d] Australian Centre for Remote Sensing, Canberra, Australia

ARTICLE INFO

Article history:
Received 31 October 2008
Received in revised form 17 June 2009
Accepted 6 July 2009

Keywords:
Remote sensing
Surface energy balance
Evapotranspiration modeling
Surface temperature
Trapezoid interpolation model
METRIC
Two-source model

ABSTRACT

Reliable estimation of the surface energy balance from local to regional scales is crucial for many applications including weather forecasting, hydrologic modeling, irrigation scheduling, water resource management, and climate change research. Numerous models have been developed using remote sensing, which permits spatially distributed mapping of the surface energy balance over large areas. This study compares flux maps over a relatively simple agricultural landscape in central Iowa, comprised of soybean and corn fields, generated with three different remote sensing-based surface energy balance models: the Two-Source Energy Balance (TSEB) model, Mapping EvapoTranspiration at high Resolution using Internalized Calibration (METRIC), and the Trapezoid Interpolation Model (TIM). The three models have different levels of complexity and input requirements, but all have operational capabilities. METRIC and TIM make use of the remotely sensed surface temperature–vegetation cover relation to define key model variables linked to wet and dry hydrologic extremes, while TSEB uses these remotely sensed inputs to define component soil and canopy temperatures, aerodynamic resistances, and fluxes. The models were run using Landsat imagery collected during the Soil Moisture Atmosphere Coupling Experiment (SMACEX) in 2002 and model results were compared with observations from a network of flux towers deployed within the study area. While TSEB and METRIC yielded similar and reasonable agreement with measured heat fluxes, with root-mean-square errors (RMSE) of ~50–75 W/m^2, errors for TIM exceeded 100 W/m^2. Despite the good agreement between TSEB and METRIC at discrete locations sampled by the flux towers, a spatial intercomparison of gridded model output (i.e., comparing output on a pixel-by-pixel basis) revealed significant discrepancies in modeled turbulent heat flux patterns that were largely correlated with vegetation density. Generally, the largest discrepancies, primarily a bias in *H*, between these two models occurred in areas with partial vegetation cover and a leaf area index (LAI) < 2.0. Adjustment of the minimum *LE* assumed for the hot/dry hydrologic extreme condition in METRIC reduced the bias in *H* between METRIC and TSEB, but caused a significant increase in bias in *LE* between the models. Spatial intercomparison of modeled flux patterns over a variety of landscapes will be required to better assess uncertainties in remote sensing surface energy balance models, and to work toward an improved hybrid modeling system.

Published by Elsevier B.V.

1. Introduction

Accurate characterization of surface energy fluxes and evapotranspiration (ET) over a range of spatial and temporal scales is critical for many geophysical applications. Ground-based or tower observations can provide representative values of ET for different land cover types, but such point data cannot be easily extrapolated to produce accurate maps over a landscape or region, due to natural variability in physical properties such as soil moisture and vegetation type. To address this need, there has been a major effort over the past several years to develop and refine remote sensing-based energy balance models that provide spatially distributed ET maps operationally using satellite data (Glenn et al., 2007; Gowda et al., 2008; Kalma et al., 2008). A few of these have been promoted as having operational capabilities.

* Corresponding author at: USDA-ARS Hydrology & Remote Sensing Lab, 10300 Baltimore Ave, Bldg 007 BARC-West, Beltsville, MD 20705-2350, USA. Tel.: +1 301 504 8498; fax: +1 301 504 8931.
E-mail address: Bill.Kustas@ars.usda.gov (W.P. Kustas).
[1] Formally at U.S. Department of Agricultural, Agricultural Research Service, Hydrology and Remote Sensing Laboratory, Beltsville, MD 20705, USA.

0168-1923/$ – see front matter. Published by Elsevier B.V.
doi:10.1016/j.agrformet.2009.07.002

One is the Trapezoid Interpolation Model (TIM), which uses land surface radiometric temperature (T_R)–vegetation index space to adjust the Priestley–Taylor based potential ET algorithm for mapping actual ET (Jiang and Islam, 2001; Batra et al., 2006; Wang et al., 2006). TIM was identified as a promising technique having little complexity and few data input requirements, yet producing reasonable ET estimates over the U.S. Southern Great Plains (Jiang and Islam, 2001; Batra et al., 2006; Wang et al., 2006) and the Senegal River basin in Africa (Stisen et al., 2008).

The Mapping EvapoTranspiration with Internalized Calibration (METRIC; Allen et al., 2007a,b) uses the principle of surface energy balance to scale sensible and latent heating between hydrologic and thermal extremes (wet/cold and dry/hot) identified within the modeling domain. Following the Surface Energy Balance Algorithm for Land (SEBAL; Bastiaanssen et al., 1998, 2005), METRIC assumes that the near-surface vertical air temperature gradient and the associated sensible heat flux relationship scale linearly with radiometric surface temperature, and latent heat is determined as a residual to the surface energy budget. The METRIC approach has been applied extensively in irrigated agricultural regions in southern Idaho, New Mexico, Colorado, Nebraska, and southern California and has been recognized as an operational approach providing spatially distributed ET over a variety of agricultural areas (Allen et al., 2007b; Kjaersgaard et al., 2008).

In comparison with TIM and METRIC, the Two-Source Energy Balance (TSEB) model contains a more detailed treatment of the radiative and turbulent heat exchange between soil and vegetation components and the soil–plant–atmosphere interface (Kustas and Norman, 1999; Kustas et al., 2004; Li et al., 2005). The TSEB partitions surface temperature and fluxes into soil and canopy components based on the local cover fraction and surface roughness characteristics. Because it does not require user intervention to subjectively select hot and cold scene end members, in contrast with METRIC and TIM, the TSEB algorithm can be fully automated has been integrated into the regional Atmosphere Land Exchange Inverse (ALEXI) model for routine monitoring of ET and drought at continental scales (Anderson et al., 2007a,b).

Although these three models have different levels of complexity, ancillary data requirements, and sensitivity to the required inputs, each requires measurements of surface temperature, vegetation cover, and standard meteorological data (primarily wind speed, air temperature, vapor pressure and solar radiation). Each has been promoted as having operational capabilities and providing robust ET estimates, as supported by comparisons with surface flux observations.

While such validation efforts using ground-based ET observations over a range of field conditions are important, very few studies have attempted to intercompare energy balance model output in order to quantify and gain greater insight as to the possible uncertainty in ET estimation across a landscape comprised of a wide variety of vegetation cover and moisture conditions (French et al., 2005; Timmermans et al., 2007).

French et al. (2005) conducted a comparison of surface energy flux maps from the TSEB and SEBAL models using an Advance Spaceborne Thermal Emission and Reflection Radiometer (ASTER) 90 m resolution T_R image over the Soil Moisture Atmosphere Coupling Experiment (SMACEX) site, a corn and soybean production region in Iowa. They pointed out that there were systematic differences between models with generally better performance from the TSEB model, while SEBAL presented difficulties in the selection of the wet and dry pixels, as the scene was primarily comprised of densely vegetated rain fed corn and soybean fields and presented no obvious minimum and maximum surface temperature endpoints.

Timmermans et al. (2007) conducted a similar type of intercomparison analysis of fluxes over heterogeneous landscapes during the SGP '97 and Monsoon '90 experiments, conducted in sub-humid grassland/winter wheat and semiarid rangeland environments, respectively. They found large discrepancies between SEBAL and TSEB flux maps over the study region, although both TSEB and SEBAL fluxes showed similar agreement with the ground observations at discrete points within the modeling domains. The greatest model discrepancies were found in areas with bare soil and sparse vegetation, which they attributed to variability in the linear relationship between surface temperature and surface-air temperature difference under heterogeneous land cover conditions.

This study compares flux estimates from the TIM, METRIC and TSEB models using remotely sensed data and ground measurements collected during SMACEX, to assess the utility and tendencies of the different modeling strategies in mapping energy fluxes. Model output is first compared with measurements from dense network of flux towers, as is often performed in model validation studies. In addition, the spatial consistency in model estimates of the energy balance components is evaluated by comparing mapped fluxes over the study region.

The SMACEX study area is a relatively simple landscape dominated by soybean and corn production, but still exhibits significant heterogeneity at the field scale in terms of fractional vegetation cover and soil moisture conditions. By comparing remote sensing-based energy balance models over an agricultural landscape that is relatively well understood and characterized, a greater understanding of the key factors directly related to model parameterizations/formulations that are driving inter-model discrepancies should emerge. The significance of the spatial differences in heat flux estimation by the different models is evaluated, and correlations of model discrepancies with specific land surface conditions are identified.

2. Study region and data

2.1. Region description

The Walnut Creek watershed (100 km^2) in Ames, IA was the main site for intensive field campaign for SMACEX from June 15 to July 8, 2002 (Kustas et al., 2005). The SMACEX campaign, providing soil, vegetation, remote sensing, and atmospheric data for investigating soil–plant–atmosphere exchange, overlapped with the Soil Moisture Experiment of 2002 (SMEX02), which focused on validation of microwave brightness temperature and soil moisture retrieval products. Full description of the region and the SMACEX campaign can be found in Kustas et al. (2005). The watershed is mainly used for row crop agriculture, with 95% of the land surface planted in corn and soybean. During the field campaign, leaf area index (LAI) ranged from ~0 to ~4 for soybean and ~0 to ~6 for corn (Anderson et al., 2004). The climate is sub-humid with an annual average rainfall of 835 mm. There were minor rainfall events a few days prior to the first Landsat overpass on June 23 (DOY 174), ranging from 0 to ~20 mm on June 20 (DOY 171), and then an extended dry down period with no rainfall observed until several days after the second Landsat overpass on July 1, DOY 182 (Kustas et al., 2005).

2.2. Ground data

Fourteen meteorological flux (METFLUX) towers were installed within the watershed (Fig. 1). Turbulent fluxes were measured at nominally 2 m above ground level in soybean fields and 4 m above ground level in corn fields, with half hourly average fluxes of sensible heat (H) and latent heat (LE), net radiation (R_N), and soil heat (G) reported. For a detailed discussion of the flux tower observations and measurement uncertainty, see Kustas et al. (2005), Prueger et al. (2005), and Meek et al. (2005). Ancillary datasets such as T_A, wind speed, and relative humidity were also

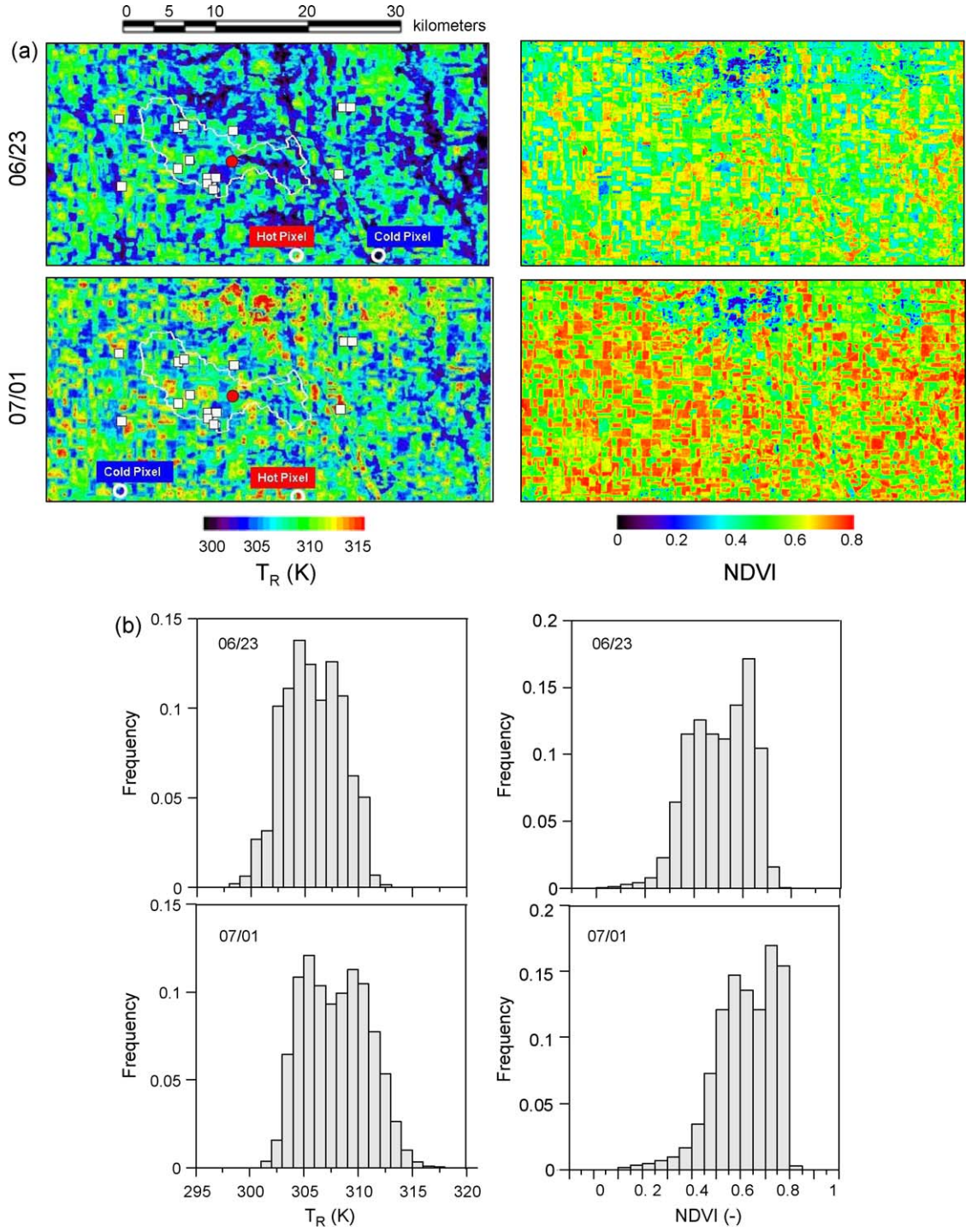

Fig. 1. (a) Surface temperature and NDVI maps for June 23 and July 01, 2002 (*Note*: white squares indicate flux tower locations, red circle indicates the location of the ID 702 weather station, and white-colored circles indicate the location of two anchor pixels used by METRIC. (b) Frequency histograms for T_R and NDVI on June 23 and July 01. (For interpretation of the references to color in this figure legend, the reader is referred to the web version of the article.)

acquired. One long-term weather station (ID 702) provided meteorological observations including T_A, solar radiation, and water vapor pressure on an hourly basis from April to August, 2002 (Fig. 1), as required by METRIC. Detailed descriptions of the flux tower and weather station measurements can also be found at http://nsidc.org/data/amsr_validation/soil_moisture/smex02/.

2.3. Remote sensing data

This study uses high-resolution thermal and visible/shortwave information from two Landsat scenes: one collected with the Landsat-5 Thematic Mapper (TM) on June 23, 2002, and a second from the Landsat-7 Enhanced Thematic Mapper Plus (ETM+) on July 1, 2002. For consistency in the comparison among models and between acquisitions, visible, near-infrared (NIR), and thermal-infrared (TIR) bands were re-sampled to a common 60-m resolution grid. Details concerning the Landsat imagery processing are given in Li et al. (2004, 2005), including atmospheric correction, re-sampling, and the determination of T_R and the Normalized Difference Vegetation Index (NDVI).

Maps of radiometric surface temperature and NDVI over the study area for the June 23 and July 1 overpasses are shown in Fig. 1,

along with associated frequency histograms. Both quantities exhibit a bimodal distribution relating to land cover, reflecting the different vegetation cover and moisture conditions that existed for the soybean and corn crops during this time frame. Vegetation cover fraction increased significantly between June 23 and July 1 due to rapid crop growth, as reflected in the increase in average NDVI in Fig. 1. It might be expected that average surface temperature would correspondingly decrease over this interval due to enhanced cooling by plant transpiration, contrary to what is observed in Fig. 1. However, surface temperatures on June 23 were likely depressed due to the rainfall event that occurred on June 20.

Empirical relationships between Landsat-derived vegetation indices and crop biophysical measurements made in the field were used along with a detailed (crop-specific) land cover classification to map LAI, vegetation cover fraction, and crop height over the watershed (Anderson et al., 2004). These site-calibrated biophysical fields were used as input to derive surface properties required by the energy balance models. While such accurate information is not generally available to operational modeling efforts, in this case we used the best available surface information to more readily isolate issues related to different model formulations from those related to errors in the model input.

3. Energy balance models

In many TIR-based surface energy balance algorithms, surface radiometric temperature is used to constrain the flux of sensible heat from the land surface by relating T_R to T_O, the aerodynamic surface temperature used in the sensible heat flux (H) equation:

$$H = \frac{(\rho C_P)T_O - T_A}{r_{AH}} \quad (1)$$

where ρ is air density, C_P is air specific heat, and r_{AH} is the aerodynamic resistance to heat transfer. Net radiation (R_N) and soil heat flux (G) are estimated from radiative transfer and canopy interception considerations (e.g., Allen et al., 2007a), then latent heat (LE) is computed as the residual of the surface energy balance equation; namely $LE = R_N - G - H$ (Jiang and Islam, 2001; French et al., 2005; Timmermans et al., 2007). As a result, LE accumulates errors from the other flux components, which may be additive or compensating.

For regional applications, flux-gradient models based on Eq. (1), require that the temperature difference, $T_O - T_A$, be accurately established for each model grid cell. The aerodynamic surface temperature is related to T_R, but the relationship depends on vegetation cover amount, canopy structure, and sensor viewing angle among other factors (Blyth and Dolman, 1995; Lhomme et al., 2000; Su et al., 2001; Kustas et al., 2007). Traditionally, the difference between T_O and T_R is mainly attributed to the fact that heat diffuses through laminar boundary layers surrounding canopy and soil elements, while momentum is transferred more efficiently as a result of viscous shear and form drag of the roughness elements involving local pressure gradients (for further discussion, see Brutsaert, 1982). Another major challenge lies in accurately specifying the required meteorological boundary conditions in T_A and accommodating inevitable biases in T_R due to inaccurate sensor calibration and atmospheric and emissivity corrections (Anderson et al., 1997; Norman et al., 1995). These difficulties have led to skepticism regarding the practical utility of thermal data in surface energy balance modeling (Hall et al., 1992; Cleugh et al., 2007). However, over the past decade a variety of methods have been developed to address these various modeling challenges for robust operational application over large areas.

3.1. Trapezoid Interpolation Model (TIM)

To circumvent issues involved in specification of T_O, r_{AH} and T_A needed in the sensible heat flux equation (Eq. (1)), Jiang and Islam (2001) proposed a simple technique to estimate LE directly, using remote sensing observations of T_R to interpolate values of a coefficient θ used in a modified Priestley–Taylor equation:

$$LE = \theta\left[(R_N - G)\frac{\Delta}{\Delta + \gamma}\right] \quad (2)$$

where γ is the psychrometric constant, and Δ is the slope of saturation vapor pressure/temperature curve at air temperature T_A (Crago and Brutsaert, 1992). The θ parameter combines the Priestley–Taylor α term and the β variable from the Budyko–Thornthwaite–Mather formulation (related to the conversion from potential evapotranspiration to actual evapotranspiration by moisture availability; Thornthwaite and Mather, 1955) to implicitly account for aerodynamic and canopy resistance. Values for θ are derived through interpolation between end member conditions, θ_{min} and θ_{max}, defined from a scatterplot of T_R vs. NDVI, which tends to assume a trapezoid-like distribution. Fig. 2 shows scatter plots in T_R–NDVI space for the Landsat 5 and 7 images on June 23

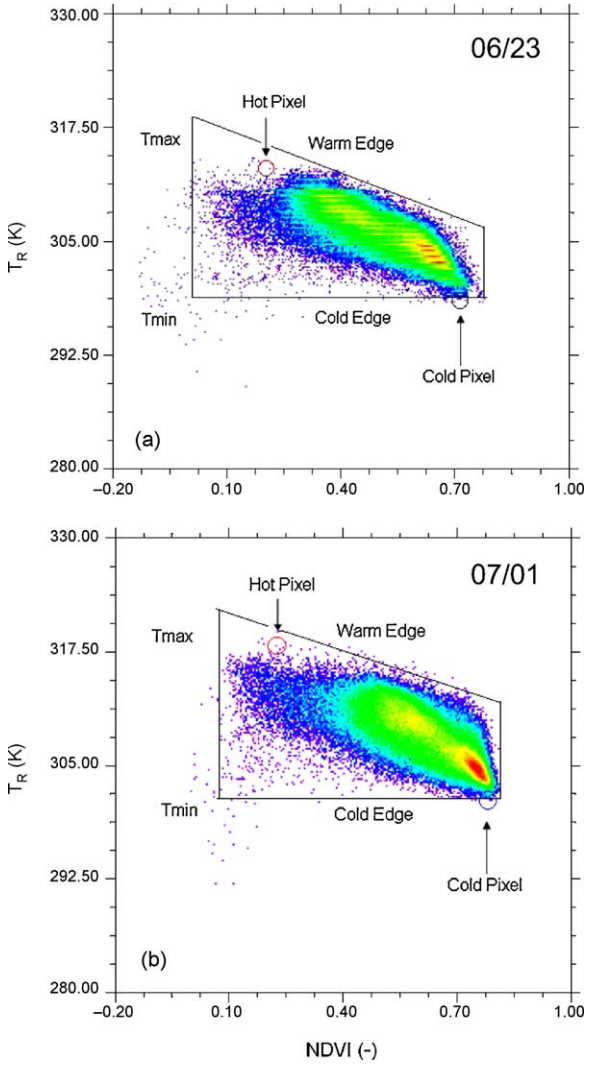

Fig. 2. Density plots for surface temperature and NDVI on June 23 and July 01, 2002 (*Note*: circles indicate hot (red) and cold (blue) endpoint pixels used in METRIC). (For interpretation of the references to color in this figure legend, the reader is referred to the web version of the article.)

and July 1, 2002 collected over the Walnut Creek watershed, IA. The boundaries of these distributions are used to define a "warm edge" indicating limiting amount of surface evaporation (θ_{min} is equal to zero) due to either a dry bare soil surface or vegetation under stressed conditions, and a "cold edge" indicating potential surface evaporation and representing wet bare soil or vegetation with ample water supply to meet atmospheric demand (θ_{max} is equal to 1.26) (Jiang and Islam, 2001). The warm and cold edges derived from the Walnut Creek study area are shown in Fig. 2; similar warm edge and cold edge equations were derived from the T_R–NDVI distribution over a larger ~100 km × 100 km regional domain. For each value of NDVI, a maximum and minimum surface temperature (T_{max} and T_{min}) is defined by these edges. The value of θ at pixel i (θ_i) is determined by interpolating the pixel temperature $T_{R(i)}$ between the two temperature limits associated with the pixel's NDVI using a procedure described by Batra et al. (2006):

$$\theta_i = \theta_{max} \frac{T_{max} - T_{R(i)}}{T_{max} - T_{min}} \quad (3)$$

While the TIM is a simple modeling system that requires minimal input data, several test applications over large heterogeneous areas have produced reasonable flux estimates (Jiang and Islam, 2001). However, the simple formulation neglects the effects of fractional vegetation, land cover, and vegetation structure on the radiometric–aerodynamic surface temperature relationship affecting H estimation (Kustas et al., 2007). Another likely limitation of the TIM approach is the requirement that a given modeling scene contains both $\theta_{min} = 0$ and $\theta_{max} = 1.26$, which may not be true for many landscapes. Furthermore, the Priestley–Taylor formulation, which represents potential ET when $\alpha = 1.26$, does not consider effects of significant local advection of energy over well-watered areas.

3.2. Mapping EvapoTranspiration at high Resolution using Internalized Calibration (METRIC) model

A modified version of the SEBAL scheme, METRIC, is fully described in Allen et al. (2007a) and briefly summarized here. In this model, potential errors in specifying $dT = T_O - T_A$ in Eq. (1) are addressed by assuming that dT scales linearly with surface temperature such that

$$dT = b + aT_R \quad (4)$$

and

$$H = \frac{(\rho c_P) dT}{r_{AH}} \quad (5)$$

where dT is the difference in air temperature between two heights $z_1 \sim 0.1$ m and $z_2 \sim 2$ m above the canopy layer, and r_{AH} is aerodynamic resistance to heat transport between these levels (s/m). The two coefficients (a and b) in Eq. (4) are derived contextually from hydrologic and vegetation cover endpoints (hot and cold pixels) contained within the scene, through examination of plots of T_R vs. NDVI (see Fig. 2). The hot pixel represents very dry conditions with near-zero ET and ideally contains no vegetation cover (low NDVI). At this pixel, $LE_{hot} \approx 0$ so $H \approx R_N - G$ and dT can be computed from Eq. (5) using an estimate of the available energy at that pixel. The cold/wet pixel ideally represents a surface with full, unstressed vegetation (high NDVI) evaporating at the reference rate ($LE_{cold} \approx ETr$) where ETr is a reference ET computed from local meteorological observations. At this endpoint, $H \approx R_N - G - LE_{cold}$ and dT is again inverted from Eq. (5). The dT and T_R values at the cold and hot pixels are then used as endpoints to establish the linear equation and coefficients in Eq. (4). At all other pixels, dT is computed with Eq. (4) based on the pixel's surface temperature. Then H is computed through an iterative process using Monin–Obukhov similarity theory to account for stability effects on r_{AH}, based on an extrapolated wind speed value at top of the surface layer, at a blending height assumed by Allen et al. (2007a) to be at $z \sim 200$ m. When H is determined, METRIC computes LE as a residual from the energy balance equation.

To compute R_N, a clear sky formulation of incoming solar radiation from Allen et al. (2007a) is used along with an albedo estimated from a weighted average of the satellite shortwave bands. Here, downwelling longwave radiation has been estimated using the Stefan–Boltzmann equation with Brutsaert's atmospheric emissivity (Brutsaert, 1975) expression, which has provided reliable estimates over a variety of landscapes and climates (Choi et al., 2008), instead of the regionally calibrated equation determined for conditions in Idaho (Allen et al., 2007a).

In METRIC, the soil heat flux G is computed as a fraction of R_N with the coefficient a function of vegetation information, albedo, α_A, and T_R:

$$\frac{G}{R_N} = (T_R - 273.15)(0.0038 + 0.0074\alpha_A)(1 - 0.98\,\mathrm{NDVI}^4) \quad (6)$$

Eq. (6) has several coefficients that are likely to vary with land cover type, but this expression was not calibrated with measurements from this study.

In this application of METRIC, locally calibrated parameters used for atmospheric correction of T_R, including path radiance, narrow band downward thermal radiation from a clear sky, and narrow band transmissivity of air, were adapted for Iowa conditions using MODTRAN 4.1 radiative transfer model (Li et al., 2004). Local weather data required by METRIC, including wind speed, air temperature, and water vapor pressure, were extracted from the ID 702 weather station located in the center of the watershed (Fig. 1). Reference evapotranspiration for alfalfa (ET_r) was estimated with the ASCE standardized Penman–Monteith method (ASCE-EWRI, 2005) using local parameters from the weather station site. For the cold pixel, a reference ET fraction ($ETrF$) value of 1.05 was used to multiply ET_r to estimate a more reliable LE_{cold} value since Allen et al. (2007a) determined that the ET is typically 5% larger than the standard ET_r value under wet soil conditions with full vegetation canopy cover. For the hot pixel, the $ETrF$ coefficient is often assumed to be zero ($LE_{hot} = 0$), but can be greater than zero when there is residual evaporation from bare soil caused by prior rain events or if there is transpiration from sparse vegetation.

The internal calibration in METRIC using ground-based reference ET has several advantages. It accommodates advective conditions where ET may exceed $R_N - G$ as argued by Allen et al. (2006, 2007a), and may provide for some adjustment to potential biases in R_N, G, roughness length, and T_R. Allen et al. (2007a) argue that assuming a diurnally constant $ETrF$ provides an improved extrapolation to daily total ET, in comparison with assuming a constant evaporative fraction. However, the selection of the hot and cold anchor pixels is subjective and the process is often not easily defined or automated. Allen et al. (2007a,b) cautioned for the need for user experience and expertise to produce high accuracy in ET. Another issue is determining an appropriate LE_{hot} value associated with the hot pixel. In METRIC, the simple daily soil water balance model described in the FAO56 publication (Allen et al., 1998, 2005) is used to estimate $ETrF$ at the hot pixel, with values typically varying between 0 and 0.1. The water balance model runs over some time interval prior to the modeling date using observed precipitation and meteorological data from the local weather station to estimate the residual moisture and ET at the time of imaging. In the scenes studied here, a variation in the

ETrF for the hot pixel from 0 to 0.1 yields a change in the average *LE* for a scene of ~5%.

It should be noted that it was not possible to locate a completely bare soil pixel for the hot pixel anchor in the sub-humid agricultural area studied here; NDVI was about 0.2 and 0.22 for the two hot pixels identified in Fig. 2. These pixels are in areas of lower cover, which are likely to be late plantings of a soybean crop As noted with the TIM implementation, the distribution of T_R vs. NDVI was similar over a larger ~100 km × 100 km domain, thus expanding the spatial domain did not alleviate this issue. The presence of even sparse vegetation cover in rain fed areas is likely to result in non-zero ET at the hot/dry pixel, potentially violating the endpoint assumption of $ETrF \sim 0$.

3.3. Two-Source Energy Balance (TSEB) model

While TIM and METRIC are interpolation schemes, using T_R as a relative indicator of where a given pixel lies between wet and dry hydrologic extremes, the TSEB model takes a more physical approach to interpreting surface temperature in relation to the surface energy balance. The basic formulation of the TSEB scheme is described in Kustas and Norman (1999) and Li et al. (2005). In contrast to one-source modeling, TSEB separates the land surface into two components: the soil surface and vegetation canopy. The TSEB partitions TIR observations at view zenith angle φ into soil and canopy contributions using the equation

$$T_R(\varphi) \approx [f_C(\varphi)T_C^4 + (1 - f_C(\varphi))T_S^4]^{1/4} \quad (7)$$

where T_C is canopy temperature, T_S is soil temperature, and $f_C(\varphi)$ is fractional vegetation cover with φ. Consequently, the sensible heat flux H from soil and vegetated canopy can be expressed as

$$H = \rho C_P \frac{T_C - T_{AC}}{r_X} + \rho C_P \frac{T_S - T_{AC}}{r_S} = \rho C_P \frac{T_{AC} - T_A}{r_A} \quad (8)$$

where T_{AC} is air temperature in canopy air space essentially representing T_O (see Kustas and Anderson, 2009), r_A is aerodynamic resistance to heat transfer between canopy and surface, r_X is total boundary layer resistance of complete canopy of leaves, and r_S is resistance of soil surface (Kustas and Norman, 1999). The surface energy budget is balanced for both the soil and canopy components of the land surface system:

$$R_N = R_{NS} + R_{NC} = H + LE + G \quad (9)$$

$$R_{NS} = H_S + LE_S + G \quad (10)$$

$$R_{NC} = H_C + LE_C \quad (11)$$

where H_S and H_C are sensible heat fluxes partitioned between soil and vegetated canopy, respectively, and R_{NS} and R_{NC} are the net radiation at the soil surface and the divergence (i.e., sink) of net radiation within the vegetation canopy layer. The latent heat flux from the vegetated canopy (LE_C) is derived from the Priestley–Taylor equation with an initial Priestley–Taylor α value of 1.26 representing a potential transpiration rate. The latent heat flux (LE_S) from soil surface is derived as a residual of energy balance model with the surface soil heat flux (G) estimated by the fraction of R_{NS} (i.e., $G \approx 0.3R_{NS}$). If LE_S is found to be negative (condensation onto the soil, which is an unlikely condition under clear daytime skies), this is interpreted as a signal that LE_C has been over-estimated and α is iteratively reduced, indicating some degree of vegetation stress.

Ancillary inputs to the TSEB include insolation, meteorological data (namely air temperature and wind speed), fractional vegetation cover, and land cover class (to determine canopy height and surface roughness). To approximate a general application of the model, where local data might not necessarily be available, domain-averaged meteorological forcing data used in TSEB (T_A and u) were generated by averaging observations over the entire SMACEX flux tower network. The variation in T_A and u among the stations at the satellite overpass times were ~0.5 °C and ~1 m/s, respectively. For comparison, the TSEB was also run using data from the long-term weather station used in the METRIC water balance model, approximating an application using local data. This modified TSEB heat fluxes by less than 25 W/m^2, a relatively minor difference in comparison with the model-to-model differences described below. In prior studies, the TSEB was also forced with meteorological data collected at ~40 m above ground level with no measurable difference in model performance relative to using data from the flux tower network (Kustas et al., 2004).

Unlike TIM and METRIC, which use the upper and lower limits of T_R and fractional vegetation cover within a scene to internally calibrate key model variables, the TSEB scheme uses these remotely sensed data as direct inputs (or in "absolute terms") in the computation of the soil, canopy and aerodynamic surface temperatures and heat flux components. As a result, the TSEB scheme has greater sensitivity to uncertainty in T_R values caused by errors in atmospheric and emissivity corrections and to errors in defining a spatially distributed air temperature field. However, it is important to note that sensitivity to errors in T_R and T_A have been greatly reduced by coupling TSEB into a time-differencing-atmosphere boundary layer growth modeling scheme initially proposed by Anderson et al. (1997) using geostationary satellite data. This modeling scheme was applied and evaluated over the SMACEX study area and its performance was similar to the local application of TSEB (Anderson et al., 2005).

4. Comparison with flux observations

For comparison with observations from the tower network, flux estimates from the three models were averaged over the estimated upwind source-area/footprint (~100 m in dimension) for each flux tower using the approach described by Li et al. (2008). As observed in many studies, the sum of the turbulent flux measurements of H and LE using the eddy covariance technique tends to be less than the available energy, $R_N - G$ (Prueger et al., 2005). Since the models assume energy balance closure ($H + LE = R_N - G$), the observed turbulent fluxes were modified to achieve closure by both the Bowen ratio (BR) and residual (RE) methods described by Twine et al. (2000). In brief, the BR method preserves the Bowen ratio (H/LE) from the eddy covariance system and partitions the remaining available energy based on this ratio while the RE method assigns any remaining available energy to LE only. The unclosed and closed flux estimates likely bracket the true turbulent fluxes from the tower footprint, and give a measure of observational uncertainty.

For both R_N and G, the three models are in reasonable agreement with the tower measurements, yielding root-mean-square error values (RMSE) of 20–30 W/m^2 and relatively small biases of 20 W/m^2 or less (Fig. 3 and Table 1). The turbulent flux estimates of H and LE exhibit larger errors, with RMSE values up to 150 W/m^2 for the TIM model (Fig. 3 and Table 1). Model performance statistics depended on the choice of the closure method applied to the tower measurements. Average RMSE values for both closed and unclosed H and LE fluxes ranged between ~30 and 90 W/m^2 using TSEB and METRIC. In general, both models performed similarly well in comparison with the tower observations, both yielding RMSE of 38 W/m^2 for all flux components combined, assuming the closure technique that optimized RMSE for each model (RE for TSEB, and BR for METRIC). The TIM approach

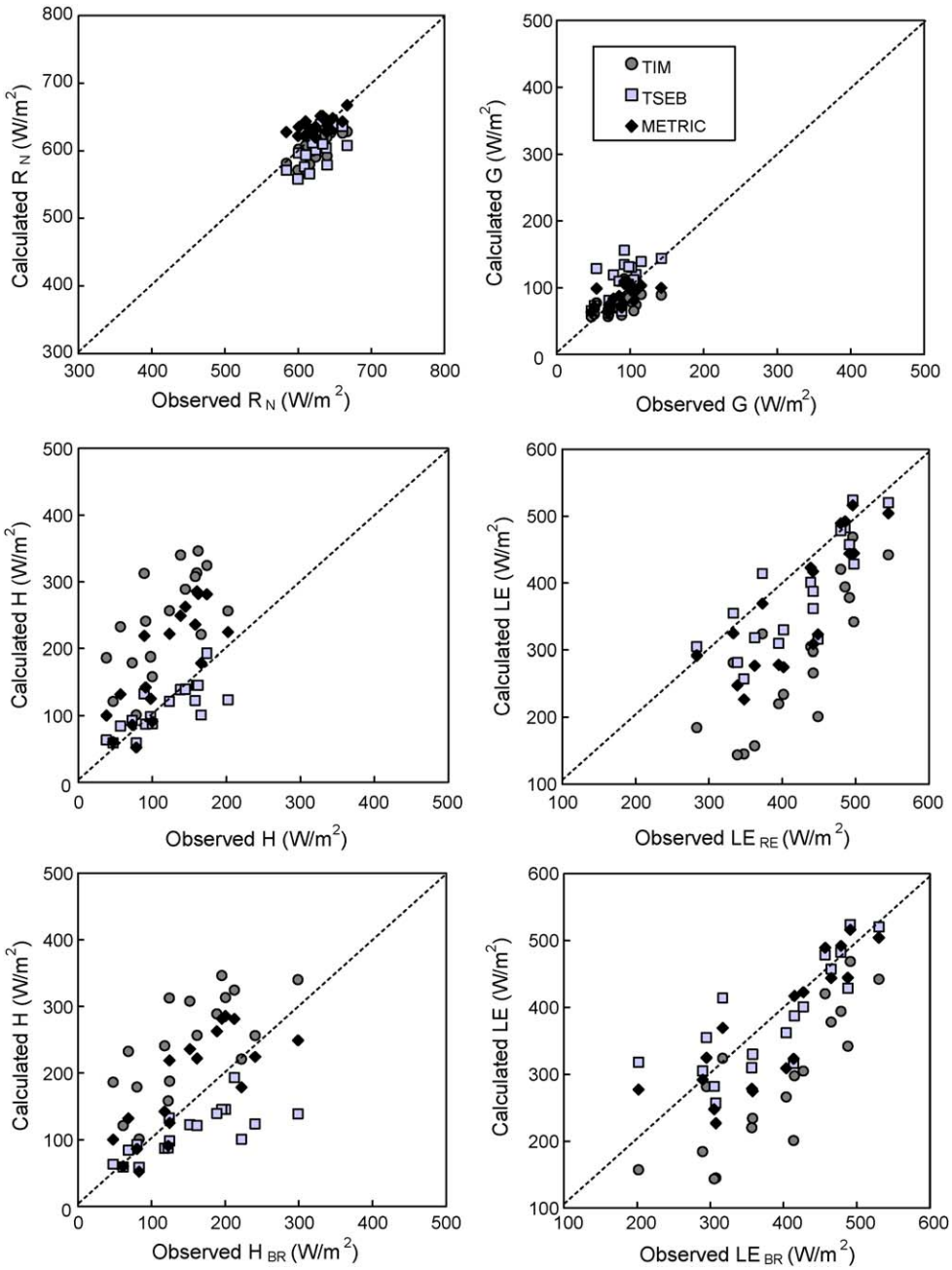

Fig. 3. Comparison between modeled and measured fluxes at the Landsat overpass time on June 23 and July 01, 2002.

Table 1
Statistics comparing modeled output and flux measurements [W/m^2] (*Note*: observed fluxes H_{BR} and LE_{BR} have been modified for energy balance closure using the Bowen ratio (BR) method, while LE_{RE} was modified using the residual (RE) closure method).

Flux component	Observed	TIM			TSEB			METRIC		
	Average	Average	RMSE	BIAS	Average	RMSE	BIAS	Average	RMSE	BIAS
R_N	627	606	26	21	606	30	21	637	19	−10
G	88	74	24	14	110	32	−22	88	19	0
H	117	243	138	−126	111	31	6	179	80	−63
H_{BR}	150	243	108	−93	111	62	39	179	57	−29
LE	314	289	65	25	385	90	−71	370	78	−55
LE_{RE}	422	289	146	133	385	60	37	370	75	53
LE_{BR}	389	289	115	−93	385	53	4	370	55	19
All flux components combined	301	291	89	−17	299	51	2	313	55	−12
All fluxes (RE closure)	314	303	84	10	303	38	11	319	48	−5
All fluxes (BR closure)	314	303	68	−38	303	44	11	319	38	−5

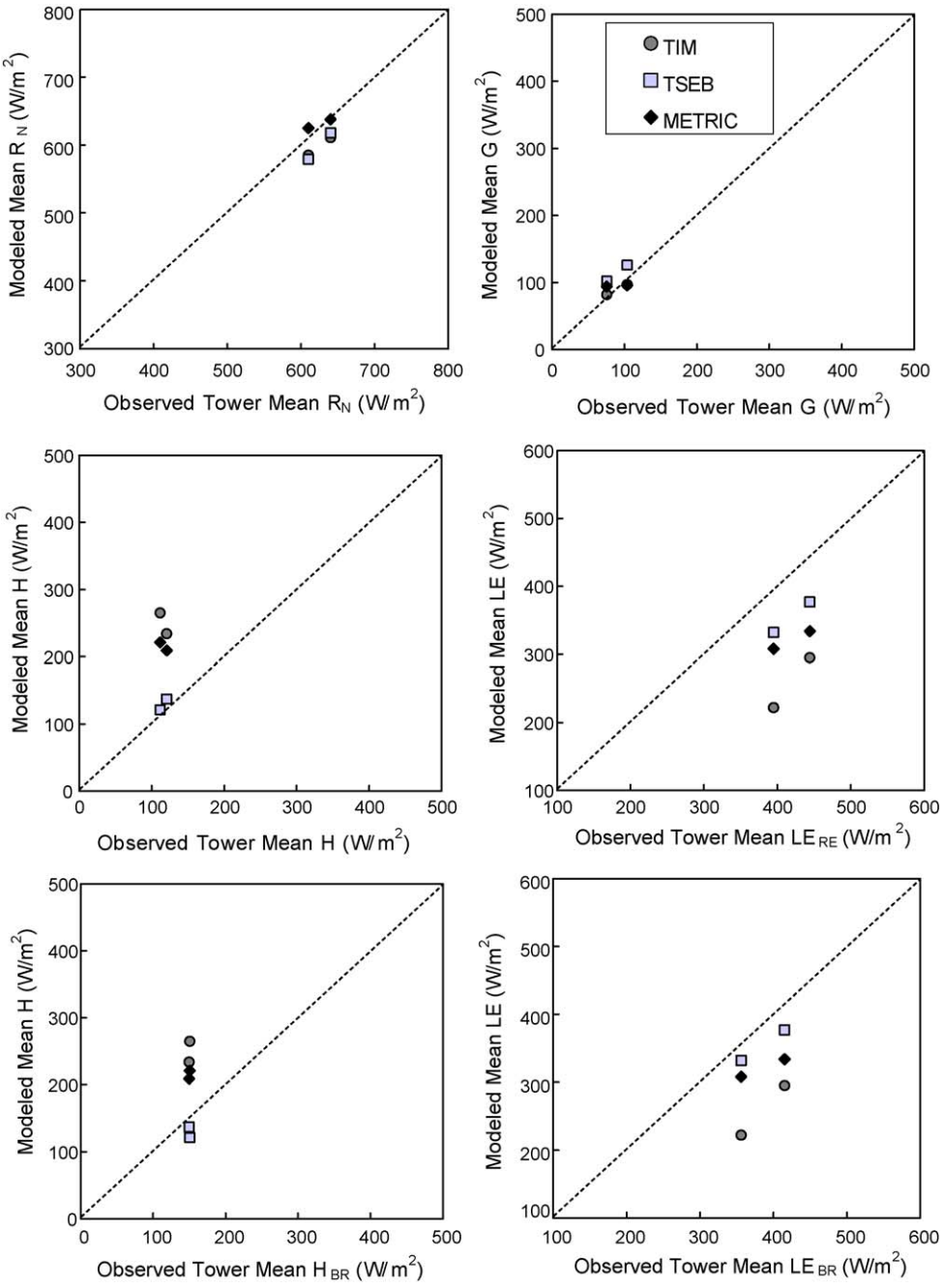

Fig. 4. Comparison between area-averaged modeled fluxes and measured fluxes from the tower network at the Landsat overpass time on June 23 and July 01, 2002.

Table 2
Difference statistics comparing flux output [W/m^2] from three surface energy balance models, taken in pairs (TIM–TSEB, METRIC–TSEB, and METRIC–TIM).

Date		06/23			07/01		
Models		TIM–TSEB	METRIC–TSEB	METRIC–TIM	TIM–TSEB	METRIC–TSEB	METRIC–TIM
R_N	Bias	6	47	41	−7	20	27
	RMSE	18	53	42	16	30	31
G	Bias	−28	−29	−1	−20	−7	12
	RMSE	39	34	24	31	19	20
H	Bias	145	100	−45	97	72	−25
	RMSE	149	114	71	106	100	64
LE	Bias	−110	−24	86	−82	−43	40
	RMSE	114	52	94	89	74	62

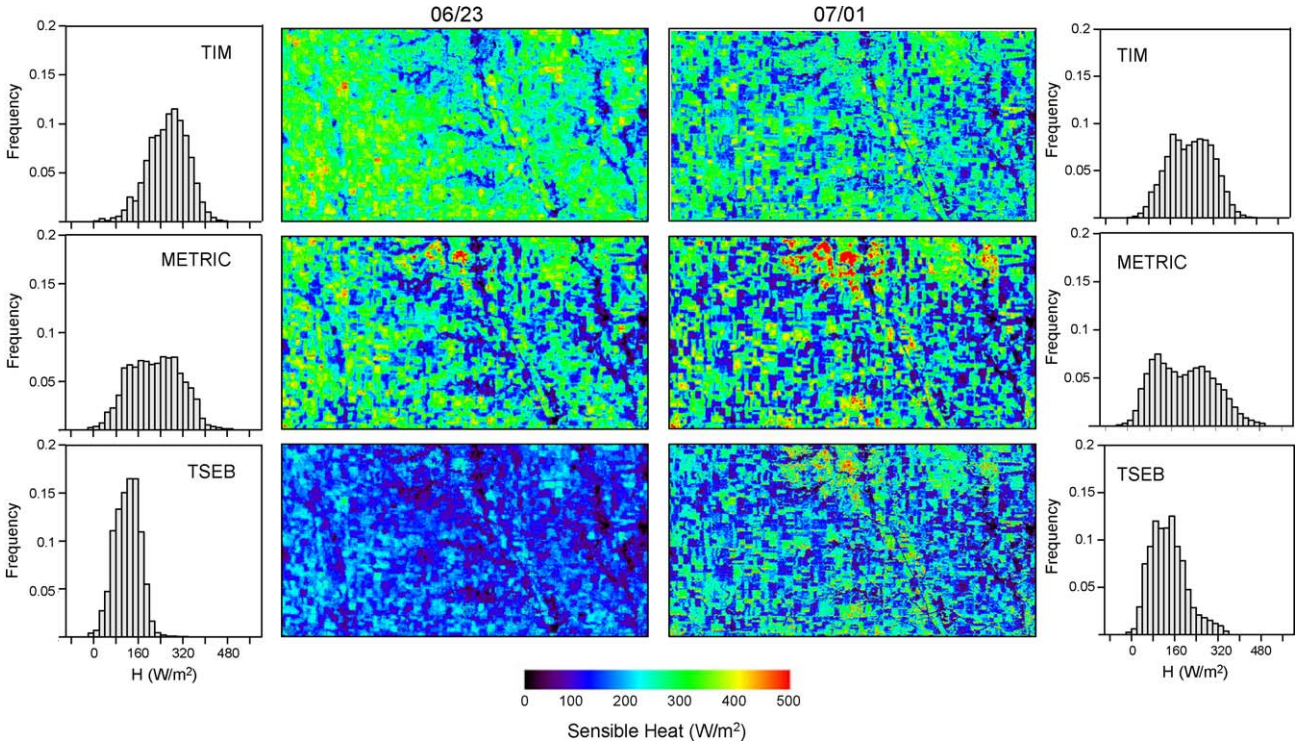

Fig. 5. Sensible heat flux (H; W/m^2) maps with frequency histograms from TIM (top), METRIC (middle) and TSEB (bottom) for June 23 (left) and July 01, 2002 (right). (For interpretation of the references to color in this figure legend, the reader is referred to the web version of the article.)

had significantly greater difficulty in reproducing individual tower fluxes, with average RMSE values exceeding 100 W/m^2.

To ascertain how well the models were able to reproduce surface fluxes at spatial scales larger than a single tower footprint, area-averaged model output over the study domain was also compared to average fluxes from the tower measurement network (Fig. 4). The network-average fluxes have been shown to be representative of the catchment scale fluxes based on comparison with aircraft flux data and model output at 5–10 km resolutions (Prueger et al., 2005; Anderson et al., 2005). The flux aircraft measurements of H and LE using the eddy covariance technique gave similar closure values compared to the tower network. Hence, flux divergence and other aircraft sampling issues, between the surface and the measurement height (~40 m) were not considered to be significant (Prueger et al., 2005). At this scale, both TIM and METRIC tend to overestimate network average H by ~115 and 80 W/m^2, respectively, and underestimate LE by 145 and 80 W/m^2 (Fig. 4). On the other hand, the TSEB technique reproduced the observed area-averaged fluxes over SMACEX with greater accuracy with differences for $H < 10$ W/m^2 and $LE < 50$ W/m^2 (Fig. 4). The

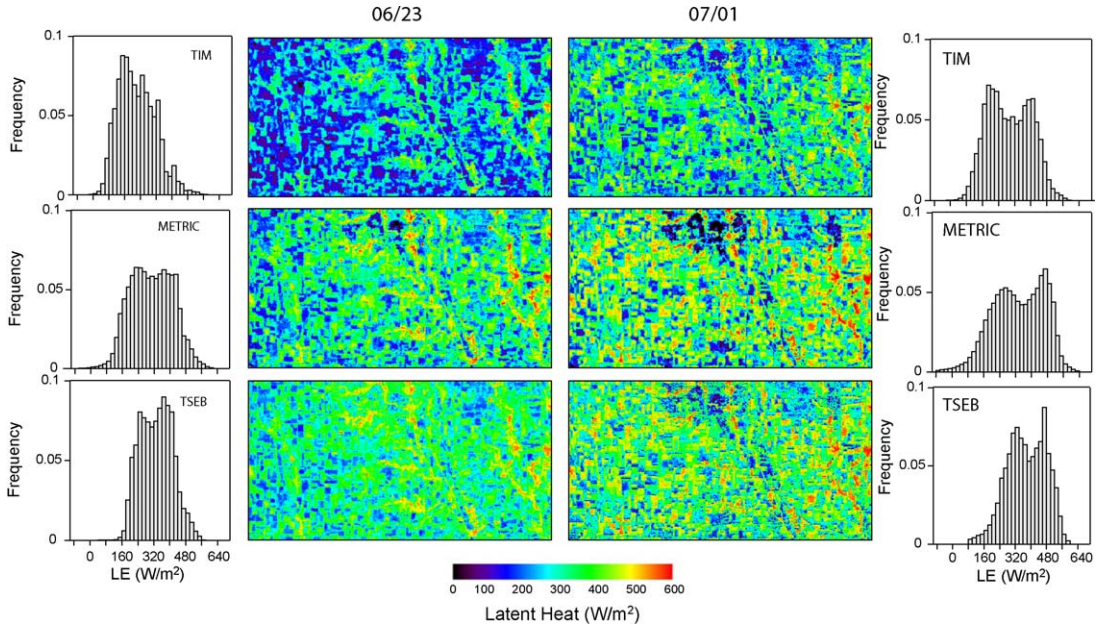

Fig. 6. Latent heat flux (LE; W/m^2) maps with frequency histograms from TIM (top), METRIC (middle) and TSEB (bottom) for June 23 (left) and July 01, 2002 (right). (For interpretation of the references to color in this figure legend, the reader is referred to the web version of the article.)

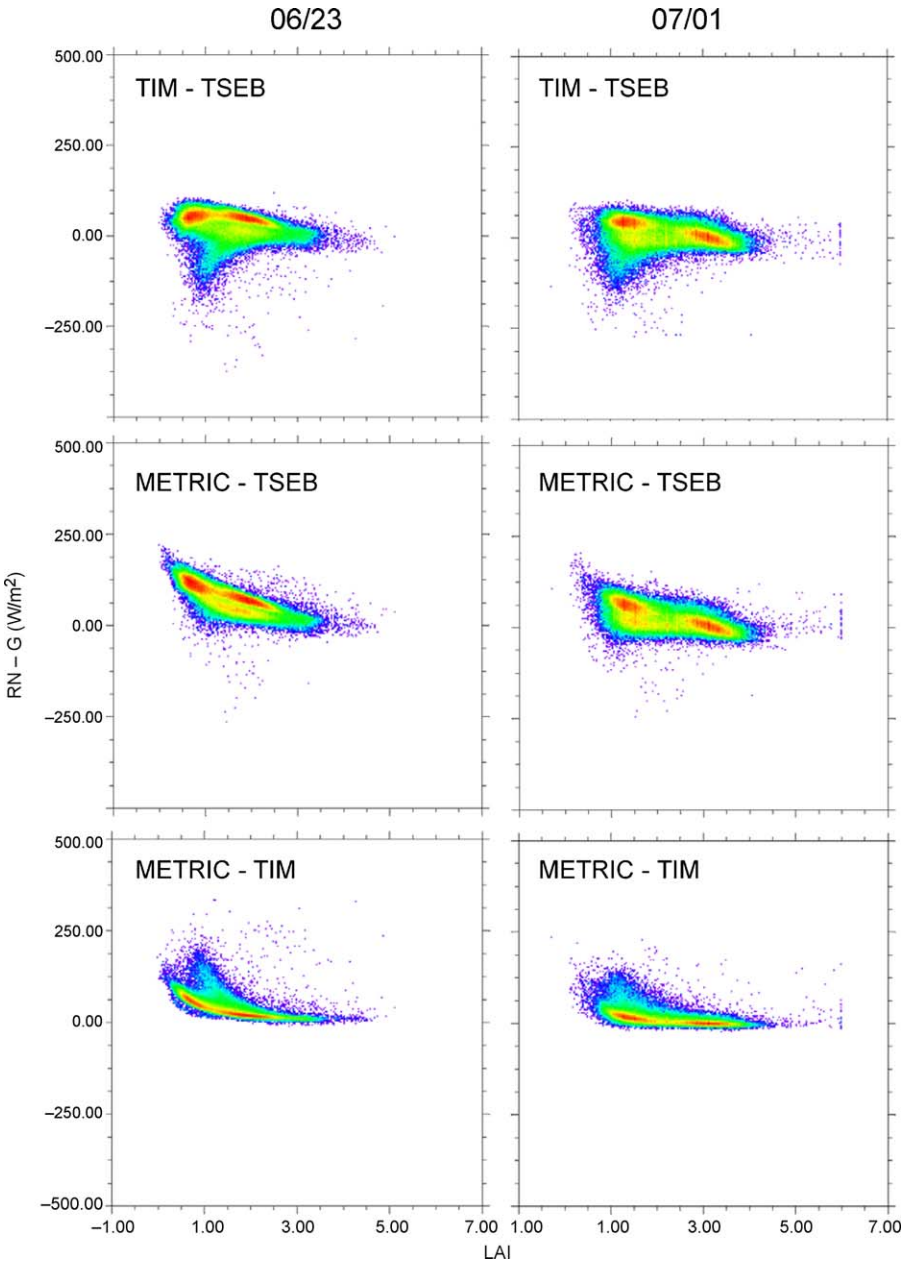

Fig. 7. Density plots of inter-model differences in available energy ($R_N - G$) vs. LAI on June 23 and July 1, 2002. (For interpretation of the references to color in this figure legend, the reader is referred to the web version of the article.)

close agreement between TSEB and tower-averaged fluxes was also demonstrated by Kustas et al. (2004) and Anderson et al. (2005).

5. Model intercomparison

Validation of model output with a handful of tower flux measurements is often used to assess the utility of energy balance models. However, this type of point-based comparison does not guarantee the model provides reliable fluxes over the full range of surface conditions that can exist across a landscape (Timmermans et al., 2007). Therefore a spatial (pixel-by-pixel) intercomparison of surface flux fields generated by the TIM, METRIC and TSEB models was also conducted. Such a model intercomparison allows for investigations of landscape properties and conditions that cause significant discrepancies among the models and potentially allows for a greater understanding of the factors causing such discrepancies.

The largest differences among the models were in the turbulent fluxes, H and LE, while discrepancies in R_N and G tended to fall within a typical range of model-measurement differences. Moreover, the magnitude of differences in R_N and G for each model did not show consistent patterns for the two overpass dates (Table 2). Therefore we focus here on model differences in the turbulent fluxes.

In Fig. 5, the spatial pattern of H generated by each model is illustrated along with a histogram showing the frequency distribution of values within the modeling domain. There are noteworthy differences between the models, both in terms of overall magnitude and spatial distribution/pattern—particularly for the 23 June date where partial cover conditions were more prevalent and some residual evaporation from prior rain events was occurring. In general, the sensible heat flux maps from the TIM and METRIC models were fairly similar, while comparisons with TSEB yielded larger differences (Table 2). Both TIM and METRIC predicted a decrease in average H from June 23 to July 1, while the

domain average H from TSEB increased slightly. The time-behavior in the area-averaged flux estimates from TSEB (i.e., increased sensible heating) is well supported by the tower network observations, regardless of closure technique (Fig. 4).

For both dates, TIM and METRIC produce similar histograms of H, spanning a full range from 0 to 500 W/m^2 (Fig. 5). In contrast, the distribution in H from the TSEB peaks at smaller values and is constrained over a narrower range, extending up to only 250–300 W/m^2. This difference in behavior is due to the fact that both TIM and METRIC assume a full or nearly full range in hydrologic conditions (i.e., $H \approx 0$ to $H \approx R_N - G$) existed within the study area/scene, forcing an interpolation of H values over this entire range. In contrast, the TSEB scheme does not make any assumption about hydrologic endpoints. French et al. (2005) found similar restriction of the flux range using TSEB compared to SEBAL.

Latent heat flux distributions from all models show a bimodal pattern (Fig. 6), reflecting the large difference in average LAI for corn and soybean crops in the area. Histograms for LE (Fig. 6) are more similar between models than those for H (Fig. 5).

The scatter plots in Figs. 7–9 demonstrate the correlation of inter-model flux differences with vegetation cover amount, as defined by the leaf area index (LAI), revealing consistent patterns for both imaging dates. For $R_N - G$, the models differ most significantly at LAI < 2, with a weaker trend at higher values of LAI (Fig. 7). For the METRIC–TSEB comparisons, the larger discrepancies in $R_N - G$ at lower LAI is due primarily to differences in R_N and more specifically to the model parameterization of shortwave albedo. In METRIC, the shortwave albedo is computed from a weighted average of the different visible and near-infrared bands from the Landsat sensors. The TSEB scheme uses an analytical formalism describing light interception by canopies described by Campbell and Norman (1998) and Anderson et al. (2000). This involves specification of leaf absorptivity and soil reflectance in the visible and near-infrared wavebands, where the bulk soil-canopy albedo is computed as a radiation-weighted average of diffuse and direct beam reflectance factors that depend on fractional vegetation cover. As a result, a narrower range in the bulk shortwave albedo is estimated using the TSEB formulation,

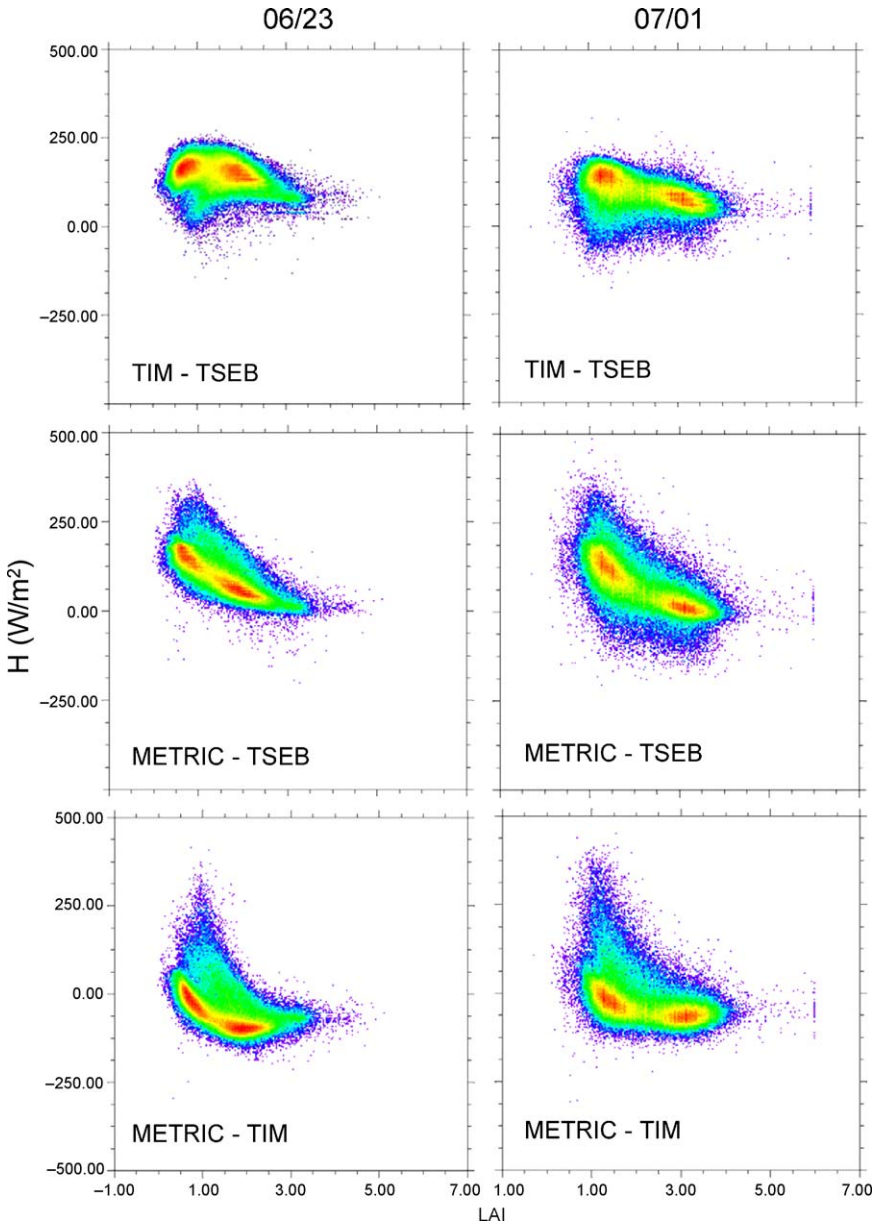

Fig. 8. Density plots of inter-model differences in sensible heat (H) vs. LAI on June 23 and July 1, 2002. (For interpretation of the references to color in this figure legend, the reader is referred to the web version of the article.)

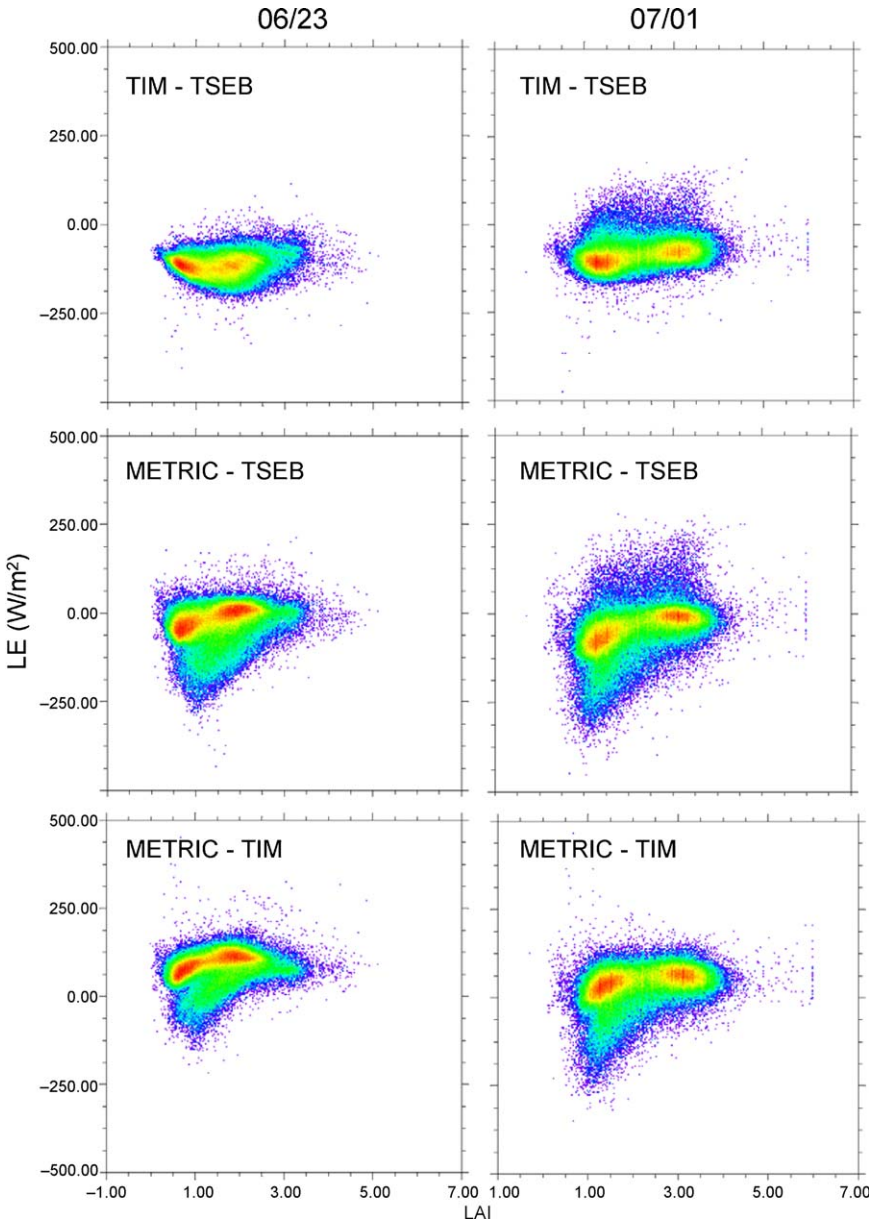

Fig. 9. Density plots of inter-model differences in latent heat (*LE*) vs. LAI on June 23 and July 1, 2002. (For interpretation of the references to color in this figure legend, the reader is referred to the web version of the article.)

particularly for the low cover conditions where there is a tendency for the METRIC soil albedo values to be lower than those specified in TSEB.

A much stronger and consistent trend emerges when model differences in H are plotted as a function of LAI, with discrepancies decreasing as LAI increases (Fig. 8). This is particularly evident between TSEB and METRIC, although there are slight trends for TIM–TSEB and METRIC–TIM. There is a significant bias, particularly for LAI < 2 with both TIM and METRIC model output having H values often greater by >100 W/m^2 compared to the TSEB model values. Model difference plots for LE (Fig. 9) mirror the trends in H (Fig. 8), but with somewhat smaller biases due to compensating model disparities in $R_N - G$ (Fig. 7). Similar biases were detected by French et al. (2005) in comparing SEBAL with TSEB output, although with lesser compensatory effects of $R_N - G$ on LE (see Fig. 5 in French et al., 2005).

To gain some insight into to what factor(s) are causing these differences between model output fields, scatter plots comparing fluxes from two of the models, METRIC and TSEB, are shown in Fig. 10 for pixels containing the two main land cover types/crops present in the scene: soybean and corn. The comparison is illustrated for DOY 174 only, although the results are similar for DOY 182. The generally higher H values computed by METRIC do not result in significantly lower LE values when compared to TSEB because of counterbalancing biases in R_N and G, a behavior that is part of the METRIC design. For both crops, the inter-model bias in H is similar and quite linear, suggesting an adjustment to one of the endpoint specifications in METRIC might significantly reduce the inter-model bias.

While there appear to be pixels/areas that are representative of reference ET conditions (Fig. 2), hence permitting a reliable selection of the "cold pixel" for METRIC, the selection of "hot pixel", where ET is close to zero or some small residual value as determined from the daily water balance, was problematic in this case. As noted above, the hot pixel should ideally be representative of a dry, bare agricultural field, which was difficult to find in this corn and soybean production region at this point in the growing season, even when extending the study domain to encompass a

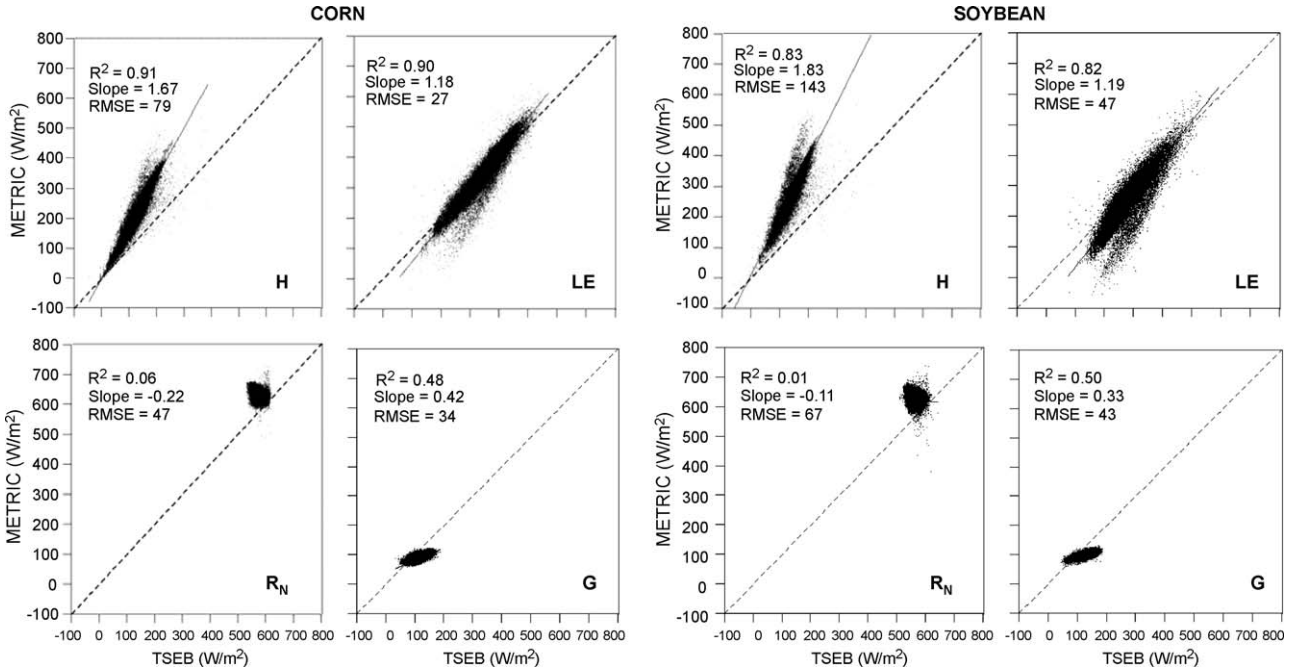

Fig. 10. Comparisons of flux estimates for *H*, *LE*, R_N and *G* from TSEB and METRIC for two main land cover types, corn (left) and soybean (right), on June 23.

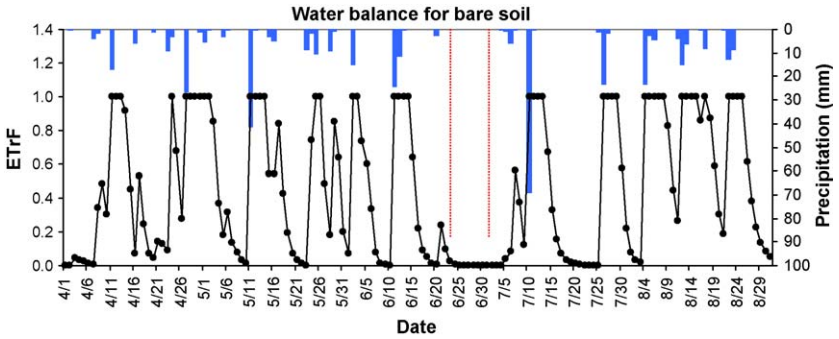

Fig. 11. Time series predictions of *ETrF* for bare soil generated by the water balance model used with METRIC for calibration of conditions at the hot/dry pixel endpoint. Also shown are daily precipitation amounts measured at weather station ID 702 (blue bars). Red lines indicate the Landsat imaging dates. (For interpretation of the references to color in this figure legend, the reader is referred to the web version of the article.)

greater portion of the Landsat scene. Use of non-zero *ETrF* at the hot pixel was therefore justified.

In Fig. 11, the time series of the *ETrF* variable computed from the water balance model is displayed, exhibiting rapid response and decay in ET based on the local precipitation and weather conditions. While an *ETrF* value of ~0.03 on the June 23 imaging date was indicated by the water balance model, a value of 0.1 was used in the simulation as recommended by Allen (personal communication, 2008) based on recent experience in applying METRIC to agricultural areas where a bare dry soil pixel in the scene is not available (see also Tasumi et al., 2005). Comparisons with the TSEB, however, indicate a larger value may have been appropriate, to better match the area-averaged sensible heat flux observed across the model domain with the tower network and flux aircraft (Fig. 4).

The sensitivity of the METRIC estimates of *H* and *LE* for corn and soybean pixels to different choices of *ETrF* at the hot pixel (referred to as $ETrF_{hot}$) is exhibited in Fig. 12, varying from 0 to 0.5 in increments of 0.1. For sensible heat, the agreement between the models decreases for both land cover types as $ETrF_{hot}$ increases, with a slope close to unity for $0.4 < ETrF_{hot} < 0.5$ for corn and $ETrF_{hot} = 0.5$ for soybean. Changing $ETrF_{hot}$, by this amount, however, clearly increases the bias in *LE* between METRIC and TSEB for both crops, because *LE* is computed as a residual to the overall energy balance and therefore absorbs the systematic changes in *H*. Given the differences in $R_N - G$ between METRIC and TSEB, there is no value of $ETrF_{hot}$ that gives consistent estimates of both *LE* and *H* between the models. For July 1 (not shown), the best agreement in *H* between models occurs when $ETrF_{hot} \sim 0.2$ for corn and 0.4 for soybean. However, as for the June 23 date (Fig. 12), use of higher *ETrF* values in METRIC for $ETrF_{hot}$ results in significant deterioration in the agreement in *LE* between METRIC and TSEB.

When the TSEB-derived $R_N - G$ field is used in METRIC, an $ETrF_{hot}$ of ~0.4–0.5 and ~0.2–0.4 for the June 23 and July 1, respectively leads to reasonable agreement in both *H* and *LE* between the two models. However, this suggests that for the hot endpoint pixel, which had sparse vegetation (NDVI ~ 0.2), the residual evaporation was 40–50% of the alfalfa reference values computed using the Penman-Monteith equation. This does not seem physically plausible. Clearly, $ETrF_{hot} > 0$ is expected for this region since NDVI values for the hot pixels (~0.2) on both overpass dates indicate the presence of partial vegetation cover. Tasumi et al. (2005) derived a relationship between *ETrF* and NDVI under dry soil moisture conditions that suggests the value of $ETrF_{hot}$

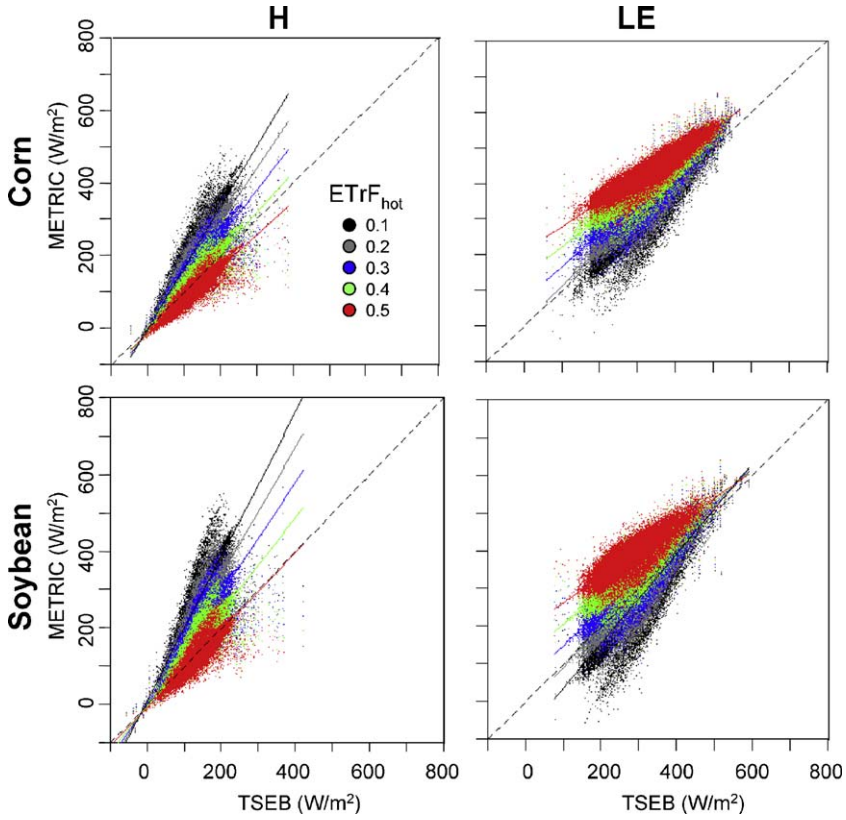

Fig. 12. Sensitivity of METRIC-derived *H* and *LE* to variations in $ETrF_{hot}$ from 0.1 to 0.5 in increments of 0.1 in comparison with TSEB fluxes for corn and soybean on June 23. (For interpretation of the references to color in this figure legend, the reader is referred to the web version of the article.)

should range from ~0.10 to 0.15 for the NDVI values at the selected hot pixel locations in the image. In summary, there does not appear to be a physically justifiable value of $ETrF_{hot}$ that leads to agreement between TSEB and METRIC fluxes, even accounting for differences in available energy predicted by the two models.

This analysis illustrates the importance of identifying a true, representative 'hot pixel' in the METRIC or SEBAL-type model and the importance of assigning the proper non-zero $ETrF_{hot}$ value to that pixel if it is not both completely dry and devoid of vegetation. It also demonstrates that in residual methods for computing latent heat (such as TSEB and METRIC), biases in *H* do not necessarily translate to an equal and opposite bias in *LE* because of the potential for a compensating bias in the available energy term (cf. Fig. 10).

6. Summary and conclusions

An intercomparison of three remote sensing-based surface energy flux models was conducted using Landsat 5 and 7 data collected over a corn and soybean production region in central Iowa during SMACEX. For R_N and *G*, there was reasonable agreement with the flux tower measurements resulting in RMSE values of 20–30 W/m^2 for the three models. However, *H* and *LE* from the three models showed greater scatter and more significant bias, with RMSE values from the TIM model reaching nearly 150 W/m^2. When model output of *H* and *LE* was averaged over the entire study domain and compared to average fluxes from the tower network, TIM and METRIC flux estimates were significantly biased, while TSEB better reproduced mean observed flux conditions. This may be related to the fact that METRIC and TIM force the predicted flux distributions to scale between wet and dry hydrologic extremes, which may not necessarily be present in every scene. TSEB does not make this assumption, and can therefore be applied to scenes with limited moisture variability. This forced scaling was also reflected in histograms of flux values generated by TIM and METRIC, which showed broader distributions than did TSEB fluxes.

The magnitude of the discrepancies among the models was identified to be strongly related to the fractional vegetation cover/LAI. In most cases, the largest differences, particularly in *H*, were observed over partially vegetated areas having LAI < 2. Model differences in available energy, $R_N - G$, tended to modulate the discrepancies in *LE*. Focusing on METRIC and TSEB, both of which showed reasonable agreement with tower fluxes, inter-model biases in *H* were found to be significant and strongly linear. An adjustment to the *ETrF* value in METRIC for the 'hot pixel condition' from ~0.1 estimated from the water balance model to 0.4–0.5 largely eliminated the bias in *H*, but served to increase the bias in LE due to model differences in available energy. These results suggest that application of METRIC in an agricultural area with high vegetation cover, containing no areas of completely bare soil at the thermal pixel scale, requires special attention to the specification of *ETrF* at the hot pixel location, including adjustment of minimum ET based on the vegetation amount in addition to residual evaporation from soil.

The model intercomparison presented here suggests that significant discrepancies in flux mapping exist among these proposed operational approaches. This was even the case for METRIC and TSEB modeling schemes, although comparisons with individual tower-based flux observations yielded satisfactory results. This SMACEX site was selected for this preliminary intercomparison because of the relative simplicity of the land surface and because important surface characteristics (e.g., land cover type, crop height, LAI) have been well-characterized using ground and satellite observations. As such this helped to isolate the key factors that affect model agreement.

While it is beyond the scope of the current study to reconcile these model discrepancies, further TSEB–METRIC intercomparisons are planned over more complex and heterogeneous landscapes, including areas with low vegetation cover where the models tend to have the largest discrepancies in heat flux estimation. Efforts to improve consistency in available energy retrieval across model implementations will enhance intercomparability of turbulent flux estimates. If this can be achieved, these intercomparison studies should ultimately lead to improvements in the algorithms used by the various models and perhaps lead to the development of a hybrid remote sensing-based energy balance/ET model with significantly greater utility and portability.

Acknowledgements

This research would not have been possible without support of the USDA-ARS Beltsville Area and NASA funding of the SMEX02/SMACEX projects. Additionally we are grateful for the technical assistance provided by Drs. Rick Allen and Jeppe Kjaersgaard, which has been critical in guiding our development and implementation of METRIC to the satellite imagery used in the current study.

References

Allen, R. G., Pereira, L. S., Raes, D., Smith, M. (1998). Crop evapotranspiration: guidelines for computing crop water requirements. United Nations FAO, Irrigation and Drainage, NY, Paper No. 56. http://www.fao.org/docrep/X0490E/X0490E00.htm.

Allen, R.G., Pereira, L.S., Smith, M., Raes, D., Wright, J.L., 2005. FAO-56 dual crop coefficient method for estimating evaporation from soil and application extensions. J. Irrigation Drain. Eng. ASCE 131 (1), 2–13.

Allen, R.G., Tasumi, M., Trezza, R., 2006. Benefits from tying satellite-based energy balance to ground-based reference evapotranspiration. International Conference on Earth Observation for vegetation monitoring and water management, Naples, Italy, 10-11 Nov. 2005, AIP Conference Proceedings 852, ISBN 0-7354-0346-5.

Allen, R.G., Tasumi, M., Trezza, R., 2007a. Satellite-based energy balance for Mapping Evapotranspiration with Internalized Calibration (METRIC)-model. J. Irrigation Drain. Eng. 133 (4), 380–394.

Allen, R.G., Tasumi, M., Morse, A., Trezza, R., Wright, J.L., Bastiaanssen, W., Kramber, W., Lorite, I., Robison, C.W., 2007b. Satellite-based energy balance for Mapping Evapotranspiration with Internalized Calibration (METRIC)-applications. J. Irrigation Drain. Eng. 133 (4), 395–406.

Anderson, M.C., Neale, C.M.U., Li, F., Norman, J.M., Kustas, W.P., Jayanthi, H., Chavez, J., 2004. Upscaling ground observations of vegetation water content, canopy height, and leaf area index during SMEX02 using aircraft and Landsat imagery. Remote Sens. Environ. 92, 447–464.

Anderson, M.C., Norman, J.M., Diak, G.R., Kustas, W.P., Mecikalski, J.R., 1997. A two-source time-integrated model for estimating surface fluxes using thermal infrared remote sensing. Remote Sens. Environ. 60, 195–216.

Anderson, M.C., Norman, J.M., Kustas, W.P., Li, F., Prueger, J.H., Mecikalski, J.R., 2005. Effects of vegetation clumping on two-source model estimates of surface energy fluxes from an agricultural landscape during SMACEX. J. Hydrometeorol. 6, 892–909.

Anderson, M.C., Norman, J.M., Mecikalski, J.R., Otkin, J.A., Kustas, W.P., 2007a. A climatological study of evapotranspiration and moisture stress across the continental United States based on thermal remote sensing: 1. Model formulation. J. Geophys. Res. 112, D10117 doi:10.1029/2006JD007506.

Anderson, M.C., Norman, J.M., Mecikalski, J.R., Otkin, J.A., Kustas, W.P., 2007b. A climatological study of evapotranspiration and moisture stress across the continental United States based on thermal remote sensing: 2. Surface moisture climatology. J. Geophys. Res. 112, D11112 doi:10.1029/2006JD007507.

Anderson, M.C., Norman, J.M., Meyers, T.P., Diak, G.R., 2000. An analytical model for estimating canopy transpiration and carbon assimilation fluxes based on canopy light-use efficiency. Agric. Forest Meteorol. 101, 265–289.

ASCE-EWRI, 2005. The ASCE standardized reference evapotranspiration equation. ASCE.EWRI Standardization of Reference Evapotranspiration Task Committe Rep., ASCE Reston, VA.

Bastiaanssen, W.G.M., Pelgrum, H., Wang, J., Ma, Y., Moreno, J., Roerink, G.J., van der Wal, T.A., 1998. A remote sensing surface energy balance algorithm for land (SEBAL). Part 2: Validation. J. Hydrol. 212–213, 213–229.

Bastiaanssen, W.G.M., Noordman, E.J.M., Pelgrum, H., Davids, G., Thoreson, B.P., Allen, R.G., 2005. SEBAL model with remotely sensed data to improve water-resources management under actual field conditions. J. Irrigation Drain. Eng. 131 (1), 85–93.

Batra, N., Islam, S., Venturini, V., Bisht, G., Jiang, L., 2006. Estimation and comparison of evapotranspiration from MODIS and AVHRR sensors for clear sky days over the Southern Great Plains. Remote Sens. Environ. 103, 1–15.

Brutsaert, W.H., 1975. On a derivable formula for long-wave radiation from clear skies. Water Resour. Res. 11 (5), 742–744.

Brutsaert, W., 1982. Evaporation into the Atmosphere: Theory, History and Applications. D. Reidel, Dordrecht, Holland, 299 pp.

Blyth, E.M., Dolman, A.J., 1995. The roughness length for heat of sparse vegetation. J. Appl. Meteorol. 34, 583–585.

Campbell, G.S., Norman, J.M., 1998. An Introduction to Environmental Biophysics. Springer-Verlag, New York, USA, 286 pp.

Choi, M., Jacobs, J.M., Kustas, W.P., 2008. Assessment of clear and cloudy sky parameterization for daily downwelling longwave radiation over different land surfaces in Florida, USA. Geophys. Res. Lett. 35, L20402 doi:10.1029/2008GL035731.

Cleugh, H.A., Leuning, R., Mu, G., Running, S.W., 2007. Regional evaporation estimates from flux tower and MODIS satellite data. Remote Sens. Environ. 106, 285–304.

Crago, R.D., Brutsaert, W., 1992. A comparison of several evaporation equations. Water Resour. Res. 28 (3), 951–954.

French, A.N., Jacobs, F., Anderson, M.C., Kustas, W.P., Timmermans, W., Gieske, A., Su, Z., Su, H., McCabe, M.F., Li, F., Prueger, J.H., Brunsell, N., 2005. Surface energy fluxes with the Advanced Spaceborne Thermal Emission and Reflection radiometer (ASTER) at the Iowa 2002 SMACEX site (USA). Remote Sens. Environ. 99, 55–65.

Glenn, E.P., Huete, A.R., Nagler, P.L., Hirschboeck, K.K., Brown, P., 2007. Integrating remote sensing and ground methods to estimate evapotranspiration. Crit. Rev. Plant Sci. 26, 139–168.

Gowda, R.H., Howell, T.A., Evett, S.R., Chavez, J.L., New, L., 2008. Remote sensing of contrasting tillage practices in the Texas Panhandle. Int. J. Remote Sens. 29 (11–12), 3477–3487.

Hall, F.G., Huemmrich, K.F., Goetz, S.J., Sellers, P.J., Nickerson, J.E., 1992. Satellite remote sensing of surface energy balance: success, failures and unresolved issues in FIFE. J. Geophys. Res. 97, 19,061–19,089.

Jiang, L., Islam, S., 2001. Estimation of surface evaporation map over southern Great Plains using remote sensing data. Water Resour. Res. 37 (2), 329–340.

Kalma, J.D., McVicar, T.R., McCabe, M.F., 2008. Estimating land surface evaporation: a review of methods using remotely sensed surface temperature data. Surv. Geophys. doi:10.1007/s10712-008-9037-z.

Kjaersgaard, J.H., Allen, R.G., Aggett, G.R., Schneider, C.A., Hattendorf, M.J., Irmak, A., Hergert, G.W., Robison, C.W., 2008. Computation of Landsat based evapotranspiration maps along the South Platte and North Platte Rivers. In: Proceedings of the 2008 World and Environmental Resources Congress of ASCE and EWRI. Honolulu, HI, May 12–16, 2008. Published on CD-ROM, ASCE 12 p.

Kustas, W.P., Anderson, M.C., 2009. Advances in thermal infrared remote sensing for land surface modeling. Agric. Forest Meteorol. 149, 2071–2081.

Kustas, W.P., Anderson, M.C., Norman, J.M., Li, F., 2007. Utility of radiometric–aerodynamic temperature relations for heat flux estimation. Bound.-Lay. Meteorol. 122, 167–187.

Kustas, W.P., Hatfield, J.L., Prueger, J.H., 2005. The Soil Moisture Atmosphere Coupling Experiment (SMACEX): background, hydrometeorological conditions, and preliminary findings. J. Hydrometeorol. 6, 791–804.

Kustas, W.P., Li, F., Jackson, T.J., Prueger, J.H., MacPherson, J.I., Wolde, M., 2004. Effects of remote sensing pixel resolution on modeled energy flux variability of croplands in Iowa. Remote Sens. Environ. 92, 535–547.

Kustas, W.P., Norman, J.M., 1999. Evaluation of soil and vegetation heat flux predictions using a simple two-source model with radiometric temperatures for partial canopy cover. Agric. Forest Meteorol. 94, 13–29.

Lhomme, J.P., Chehbouni, A., Monteny, B., 2000. Sensible heat flux–radiometric surface temperature relationship over sparse vegetation: parameterizing B^{-1}. Bound.-Lay. Meteorology 97 (3), 431–457.

Li, F., Jackson, T.J., Kustas, W.P., Schmugge, T.J., French, A.N., Cosh, M.H., Bindlish, R., 2004. Deriving land surface temperature from Landsat 5 and 7 during SMEX02/SMACEX. Remote Sens. Environ. 92, 521–534.

Li, F., Kustas, W.P., Prueger, J.H., Neale, C.M.U., Jackson, T.J., 2005. Utility of remote sensing based two-source energy balance model under low and high vegetation cover conditions. J. Hydrometeorol. 6, 878–891.

Li, F., Kustas, W.P., Anderson, M.C., Prueger, J.H., Scott, R.L., 2008. Effect of remote sensing spatial resolution on interpreting tower-based flux observations. Remote Sens. Environ. 112, 337–349.

Meek, D.W., Prueger, J.H., Kustas, W.P., Hatfield, J.L., 2005. Determining meaningful differences for SMACEX eddy covariance measurements. J. Hydrometeorol. 6, 805–811.

Norman, J.M., Divakarla, M., Goel, N.S., 1995. Algorithms for extracting information from remote thermal-IR Observations of the earth's surface. Remote Sens. Environ. 51, 157–168.

Prueger, J.H., Hatfield, J.L., Kustas, W.P., Hipps, L.E., Macpherson, J.I., Neale, C.M.U., Eichinger, W.E., Cooper, D.I., Parkin, T.B., 2005. Tower and aircraft eddy covariance measurements of water vapor, energy, and carbon dioxide fluxes during SMACEX. J. Hydrometeorol. 6, 954–960.

Stisen, S., Sandholt, I., Nørgaard, A., Fensholt, R., Jensen, K.H., 2008. Combining the triangle method with thermal inertia to estimate regional evapotranspiration—applied to MSG-SEVIRI data in the Senegal River basin. Remote Sens. Environ. 112, 1242–1255.

Su, Z., Schmugge, T., Kustas, W.P., Massman, W.J., 2001. An evaluation of two models for estimation of the roughness height for heat transfer between the land surface and the atmosphere. J. Appl. Meteorol. 40, 1933–1951.

Tasumi, M., Allen, R.G., Trezza, R., Wright, J.L., 2005. Satellite-based energy balance to assess within-population variance of crop coefficient curves. J. Irrigation Drain. Eng. ASCE 131 (1), 94–109.
Thornthwaite, C.W., Mather, J.R., 1955. The water balance. Publ. Climatol. 8 (1), 1–86.
Timmermans, W., Kustas, W.P., Anderson, M.C., French, A.N., 2007. An intercomparison of the surface energy balance algorithm for land (SEBAL) and the two-source energy balance (TSEB) modeling schemes. Remote Sens. Environ. 108, 369–384.
Twine, T.E., Kustas, W.P., Norman, J.M., Cook, D.R., Houser, P.R., Meyers, T.P., Prueger, J.H., Starks, P.J., Wesely, M.L., 2000. Correcting eddy-covariance flux underestimates over a grassland. Agric. Forest Meteorol. 103, 279–300.
Wang, K., Li, Z., Cribb, M., 2006. Estimation of evaporative fraction from a combination of day and night land surface temperatures and NDVI: a new method to determine the Priestley–Taylor parameter. Remote Sens. Environ. 102, 293–305.